Article

Crystal Structure and Magnetism of Potassium-Intercalated 2,7-Dimethylnaphthalene

HPSTAR
1270-2021

Xiao-Lin Wu [1,]*, Ren-Shu Wang [2,3], Hui Yang [4], Ming-An Fu [2], Hao Lv [1], Hua-Qing Yu [1], Xiao-Jia Chen [3], Yun Gao [2] and Zhong-Bing Huang [2,]*

[1] School of Physics and Electronic-Information Engineering, Hubei Engineering University, Xiaogan 432000, China; kuerlvhao@hotmail.com (H.L.); yuhuaqing@126.com (H.-Q.Y.)
[2] Faculty of Physics and Electronic Technology, Hubei University, Wuhan 430062, China; renshu.wang@hpstar.ac.cn (R.-S.W.); fumingan163@163.com (M.-A.F.); gaoyun@hubu.edu.cn (Y.G.)
[3] Center for High Pressure Science and Technology Advanced Research, Shanghai 201203, China; xjchen@hpstar.ac.cn
[4] School of Physics and Mechanical & Electrical Engineering, Hubei University of Education, Wuhan 430205, China; hyang@hue.edu.cn
[*] Correspondence: wuxiaolin937@163.com (X.-L.W.); huangzb@hubu.edu.cn (Z.-B.H.)

Abstract: The rich physical properties of metal-intercalated polycyclic aromatic hydrocarbon materials have recently attracted considerable attention. Crystals of potassium-intercalated 2,7-dimethylnaphthalene were synthesized via solid phase reaction. The combination of XRD measurements and first-principles calculations indicated that each unit cell contains two potassium atoms and four organic molecules. Magnetization measurements revealed that the samples show a Curie paramagnetism. Theoretical calculations showed that the intercalated structure becomes metallic and has local magnetic moment. Raman spectroscopy confirmed the migration of electron from potassium 4s to carbon 2p orbital, which is the source of magnetism. Our research on naphthalene derivatives is helpful for expanding the range of novel organic magnetic materials and organic superconducting materials.

Keywords: polycyclic aromatic hydrocarbons; potassium intercalated; curie paramagnetism

1. Introduction

The polycyclic aromatic hydrocarbons (PAHs) in nature are generally obtained from the fractionation of coal tar and the aromatizing products of petroleum, which are widely concerned by chemists and environmentalists [1–7]. In the field of novel functional materials, PAHs have also shown potential value in organic electronic device [8,9] and organic photovoltaic devices [10]. In 2010, organic superconductivity with the high superconducting transition temperature (Tc) of 7 K and 18 K was discovered in picene [11], which opened the prelude to modulation of PAHs by means of metal intercalation. Metal-intercalated PAHs can exhibit ferromagnetism [12,13], antiferromagnetism [14–16], paramagnetism [17–19], or superconductivity [20–28]. In terms of geometrical structure, PAHs with novel magnetic properties can be divided generally into nonfused and fused types. The former mainly include biphenyl [20], p-terphenyl [21], p-quaterphenyl [22], p-quinquephenyl [23], etc. The latter include naphthalene [29], anthracene [17], phenanthrene [24,25], picene [11,26], pentacene [13], coronene [27], dibenzopentacene [28], and so on. Strong electron correlation is thought to be related to magnetism in these structures.

Much has been done on the traditional PAHs, and recent attention has been paid to other materials with similar structures. For example, 2,2'-bipyridine [30] similar to biphenyl and triphenylbismuth [31] similar to triphenylmethane are also superconducting after metal intercalation. In addition, the methyl modified structure of triphenylbismuth has organic superconductivity [32,33], and the phenyl modified structure of anthracene possesses π-electron weak ferromagnetism [12]. This opens a wider window to further develop metal intercalated organic materials.

While exploring the potential magnetic properties of PAHs, it is significant to study the effect of metal insertion on the structure and electronic properties of organic crystals, as well as the mechanism of magnetic production [34–36]. Crystalline K_2Pentacene and K_2Picene with Curie behavior were successfully synthesized, forming extended herringbone structures [19]. In K-intercalated rubrene ($C_{42}H_{28}$), both the decomposition of organic material and the insertion of potassium were found at the same time, which is a common feature of similar systems [37]. Hee Cheul Choi et al. calculated the energy difference Δ ($\Delta = E_{LUMO+1} - E_{LUMO}$) of 200 PAHs molecules by the computational search method, and predicted that triphenylene ($C_{18}H_{12}$) with small Δ should be organic superconductors [38].

Here, we report the magnetic property and structure information of potassium-intercalated 2,7-dimethylnaphthalene (2,7-DMN), one of the methyl derivatives of naphthalene. In each 2,7-DMN molecule, two methyl groups are connected to the 2 and 7 positions of naphthalene, respectively. Naphthalene was theoretically predicted to exhibit compensated ferromagnetism and half metallic behavior by intercalating potassium atom [29], but no local magnetic moment was observed experimentally in potassium intercalated 2,3-dimethylnaphthalene (2,3-DMN, an isomer of 2,7-DMN) [39]. We expect to change the position of the methyl group to adjust the molecular interaction and electronic structure of potassium intercalated PAHs molecular crystals, thus generating novel physical properties.

2. Experiments

Potassium metal (purity 99%) was purchased from Sinopharm Chemical Reagent (Shanghai, China). Pristine 2,7-DMN (purity 98%, GC) were purchased from Tokyo Chemical Industry (Tokyo, Japan). The potassium metal was cut into small granules carefully in glove box and was then thoroughly mixed with 0.1 g of organics according to stoichiometric ratio of 1:1. It is better to cover the potassium granules with organic powder, so as to avoid the reaction of silvery white potassium with trace H_2O or O_2 remaining in the environment, and generate a layer of deep purple stable compound on the metal surface, which affects the interaction between active potassium and organics.

The sample was enclosed into a special pre-cleaned quartz tube, vacuumed to approximately 10^{-4} Pa and sealed. The tube containing the sample was placed in the water bath of an ultrasonic machine at 80 °C for 8 h. Then, the sample quartz tube was gradually heated to 120 °C in 40 min in an annealing furnace. The furnace maintained at 120 °C for 2 days and after that cooled down slowly by −3 °C/h. This long period of heat preservation and slow cooling was to allow the alkali potassium to fully react with the organics. After the preparation process, the original white organic powder and silvery potassium turned homogeneous black, indicating the success of the intercalation experiment. The tubes were stored in the glove box until measurement.

When the sample was taken out of the tube to measure, it could be seen that there were still lumps of potassium slag at the bottom of the tube. The possible reason was that black KH was formed on the surface of the potassium block, causing the internal potassium to not completely react with 2,7-DMN. Only powdered black samples were put on corresponding sealed capillary or capsule for measurement.

The crystal structures of the samples were measured by an X-ray diffractometer (λ = 1.5418 Å, Bruker D8 Advance, Bruker Corporation, Billerica, MA, USA). The vibration information of the samples was measured by Raman spectrometer (Horiba, Kyoto, Japan) in a 633 nm laser. The magnetic properties of the samples were measured using SQUID magnetometer (Quantum Design MPMS3, San Diego, CA, USA).

The crystal and electronic structures of the samples were calculated by plane wave pseudopotential method [40]. The electron–electron and electron–ion interactions were simulated by generalized gradient approximation [41,42]. In addition, $3 \times 1 \times 3$ k-points mesh were used for structural optimization. The partial density of states was calculated using a $5 \times 3 \times 5$ k-point sampling scheme. The convergence criterion for the energy is set as 10^{-5} eV, and the convergence criterion for the maximum force is set as 0.02 eV/Å.

3. Results and Discussion

3.1. Magnetic Property of Potassium-Intercalated 2,7-DMN

Most simple PAHs such as naphthalene and biphenyl are generally diamagnetic in the absence of unpaired electrons or radical spins [43]. Pristine 2,7-DMN also exhibited weak diamagnetism with a magnitude of about -5×10^{-4} emu·Oe^{-1}·mol^{-1}, as shown in Figure S1 of Supplementary Materials, while both the two potassium-intercalated 2,7-DMN samples (labeled as K$_1$2,7-DMN-A and K$_1$2,7-DMN-B, respectively) exhibited typical Curie paramagnetism after potassium intercalation, as clearly shown in Figure 1.
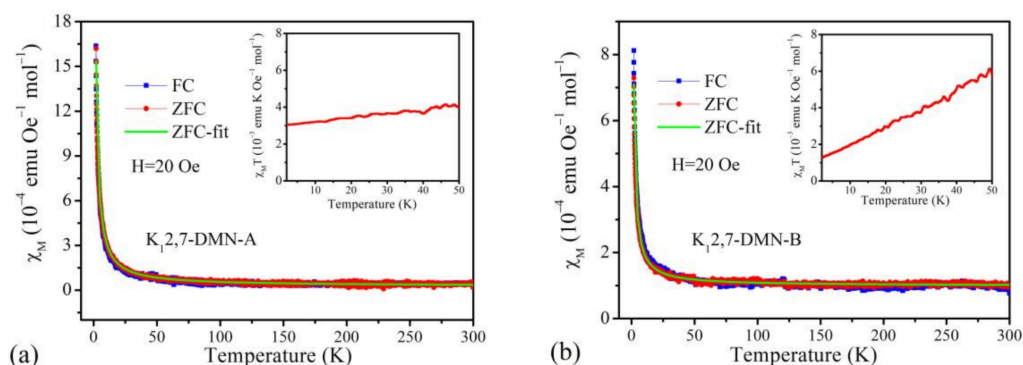

Figure 1. (**a**) The relationship between molar magnetic susceptibility (χ_M) and temperature of potassium intercalated 2,7-DMN-A sample. The inset shows the $\chi_M T - T$ curves of this sample. (**b**) The relationship between molar magnetic susceptibility and temperature of potassium intercalated 2,7-DMN-B sample. The inset shows the $\chi_M T - T$ curves of this sample.

Figure 1a exhibited the molar magnetic susceptibility (χ_M) of K$_1$2,7-DMN-A sample with temperature under 20 Oe in field cooling (FC) and zero field cooling (ZFC) conditions. With the decrease of temperature, the molar magnetic susceptibility of the sample increased inversely. The ZFC and FC data almost coincided in the whole measurement temperature rage, suggesting that the sample did not contain nonnegligible magnetic impurities. The Curie–Weiss formula ($\chi_M = \chi_{M0} + C/(T-\theta)$) is used to fit the ZFC curve, and the fitted Weiss constant (θ) of K$_1$2,7-DMN-A sample is 0.098 K, as listed in Table 1, indicating that the sample may have a tiny ferromagnetic exchange interaction.

Table 1. Curie–Weiss fitting parameters of K$_1$2,7-DMN-A and K$_1$2,7-DMN-B samples.

Sample	χ_{M0} (emu Oe^{-1} mol^{-1})	θ (K)	C (emu K Oe^{-1} mol^{-1})	M (μ_B mol^{-1})
K$_1$2,7-DMN-A	0.27×10^{-4}	0.098	28.7×10^{-4}	0.15
K$_1$2,7-DMN-B	0.99×10^{-4}	0.234	9.6×10^{-4}	0.09

The inset in Figure 1a showed the $\chi_M T - T$ curve of the K$_1$2,7-DMN-A sample. Previous literature showed that $\chi_M T$ of ferromagnetic material firstly increases and then decreases with the increase of temperature until the Curie temperature, followed by a weak temperature dependent behavior in the paramagnetic region [44], while $\chi_M T$ of antiferromagnetic material firstly increases rapidly with the increase of temperature, and then turns to increase slowly in the paramagnetic region [45]. As can be seen from the inset in Figure 1a, $\chi_M T$ of the K$_1$2,7-DMN-A sample increases almost linearly with increasing temperature, indicating that no magnetic phase transition occurs in the sample.

Figure 1b showed the magnetic data of K$_1$2,7-DMN-B sample under the same condition, which exhibited the same behavior as K$_1$2,7-DMN-A sample. One thing to note is that the molar magnetic susceptibility curves of both samples wobbled slightly at high temperature, which is due to the fact that the absolute value of the molar magnetic susceptibility at high temperature has decreased to near the measurement accuracy of the instrument

(~10^{-8}). Nevertheless, it is beyond doubt that the samples intercalated by potassium atoms exhibited completely different magnetic behavior from the original diamagnetism.

Table 1 lists the Curie–Weiss fitting parameters of $K_1$2,7-DMN-A and $K_1$2,7-DMN-B samples. Very small error values (less than 0.01 K in fitting θ) indicate that the fitting is reliable, while the magnetic moments of 0.15 and 0.09 μ_B per mole suggest that there is local magnetic moment in the intercalated materials. In the paramagnetic K_3phenanthrene and Rb_3phenanthrene samples, the experimentally observed magnetic moment is 0.2 μ_B per mole [24], and similar small magnetic moment was also found in the paramagnetic $K_{4.0}$picene sample [11].

3.2. Crystal and Electronic Structures of Potassium-Intercalated 2,7-DMN

XRD pattern of pristine and two potassium-intercalated 2,7-DMN samples were exhibited in Figure 2. Pristine 2,7-DMN sample grew in a preferred orientation with obvious peaks only located at 8.7° and 17.4° positions. After intercalation preparation, both the above peaks had a right shift of about 0.2° and new obvious peaks located at 19.6° and 28.5° appeared, suggesting that the intercalation of potassium atoms into organic molecule suppressed preferred orientation growth and caused changes in lattice parameters to form new crystal structures. KH peaks were found in samples, indicating that a small amount of potassium bonded to hydrogen in 2,7-DMN molecules to form KH. In addition, $K_1$2,7-DMN-A and $K_1$2,7-DMN-B samples were obtained with the same intercalation ratio and preparation process. The purpose of repeated preparation is to improve the persuasiveness of new structure and paramagnetic results in potassium intercalated 2,7-DMN. Of course, due to the nonuniformity of the solid phase sample and the weak signal of organic material, the experimental data of different samples are slightly different, but their new crystalline phase and magnetic properties formed after potassium intercalation are consistent.
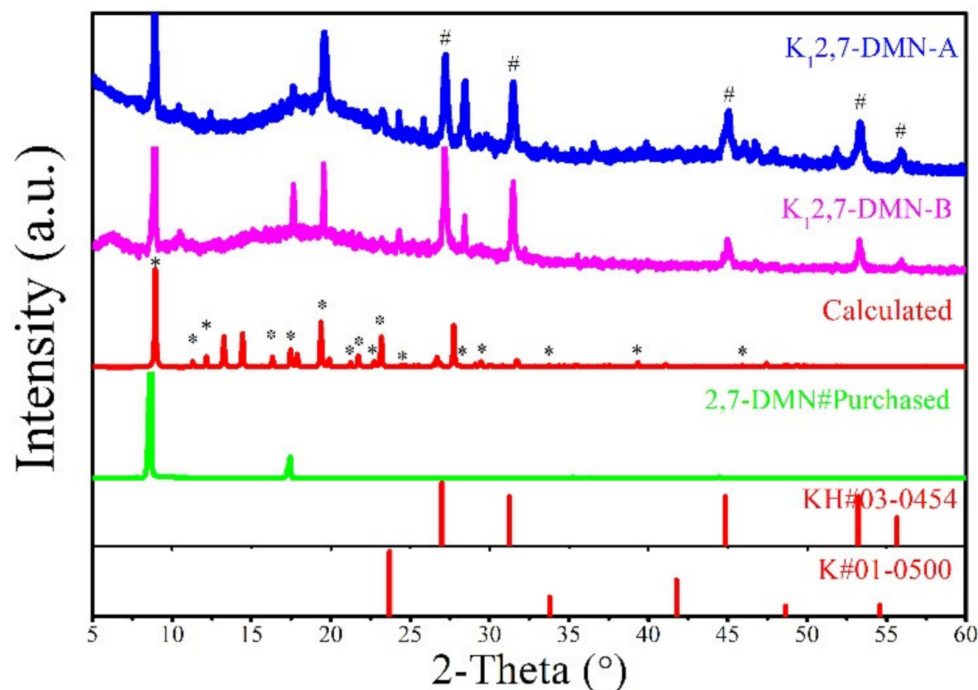

Figure 2. XRD pattern of pristine and potassium-intercalated 2,7-DMN. The symbol "#" represents the peak position of KH. "Calculated" refers to the XRD profile of the theoretical structure. The symbol "*" indicates the calculated position that coincides with the experimental curve.

The general method for searching the crystal structure of potassium-intercalated 2,7-DMN in theory is to insert potassium atoms into 2,7-DMN molecules according to the mole ratio of 1:1, 2:1 and 1:2, and relax the atomic positions sufficiently. Then, the XRD of all the

obtained stable structures (hundreds of species) are then compared with the experimental data to find the most likely structure to match the latter. It is worth noting that small fluctuations in structural parameters can also cause large changes in XRD data. Finally, a structural model is found which is in good agreement with the experimental data, which has a 1:2 ratio of potassium to organic material. Its XRD pattern is labeled as "Calculated" in Figure 2. The refined XRD data are shown in Figure S2 of the Supplementary Materials. As can be seen from the comparison of experimental and theoretical XRD data, most peak locations and relative intensities in the calculated results are close to those in the experimental data, and the small difference between the two may be caused by defects or polymorphs in the recrystallization process of intercalated samples preparation, similar to other intercalated PAHs [19,38].

Figure 3a shows the theoretical crystal structure of potassium-intercalated 2,7-DMN. In this structure, each unit cell contains two potassium atoms and four 2,7-DMN molecules. The crystal parameters are a = 6.679 Å, b = 7.819 Å, c = 19.787 Å, α = 90°, β = 92.44°, and γ = 90°, and the cell volume is 1032.4 Å^3. The positions of C, K, and H are shown in Supplementary Materials. It can be clearly seen from a 2 × 2 × 2 supercell in Figure 3a that the potassium atoms are inserted into the *b-c* plane of the organic molecules, which often leads to the expansion of these two lattice parameters [11]. In the crystal unit cell, the distance between potassium and the nearest neighbor carbon atom is about 2.51 Å, falling in between the ionic bond length (2.15 Å) and the covalent bond length (2.73 Å). This indicates that the interaction between potassium and 2,7-DMN is a mixture of ionic and covalent characters. Here, we assume that the ionic and covalent radii of potassium are 1.38 and 1.96 Å, respectively, and the radius of carbon is 0.77 Å.

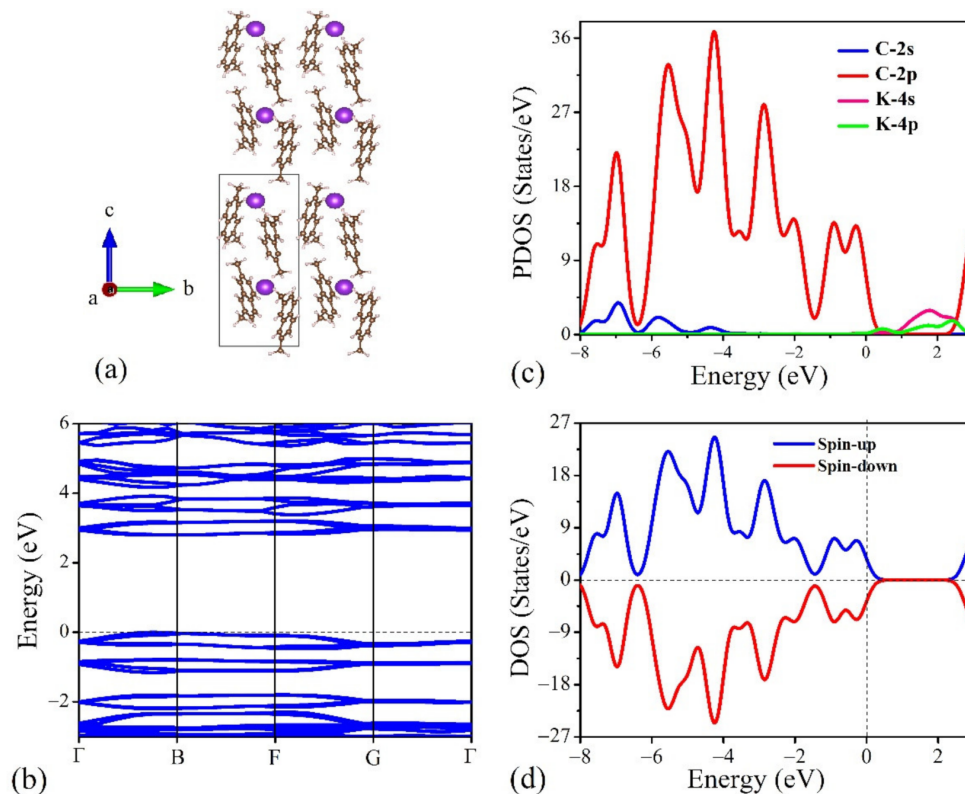**Figure 3.** (**a**) The calculated potassium-intercalated 2,7-DMN structure is shown in a 2 × 2 × 2 supercell. The purple balls represent potassium atoms, and the brown balls represent carbon atoms. (**b**) The band of the theoretical model. (**c**) The relationship between Orbital-resolved partial density of states (PDOS) and the energy of theoretical model. (**d**) The relationship between spin-dependent density of states (DOS) and the energy of theoretical model.

The energy of the ferromagnetic and antiferromagnetic configurations was calculated based on the theoretical model. The results show the energy of ferromagnetic configuration is less than 1 meV lower than that of antiferromagnetic configuration, indicating that the intermolecular magnetic exchange interaction is very small, which is responsible for the Curie paramagnetism of samples. The molecular magnetic moment was also calculated for the ferromagnetic configuration. The magnetic moment range of carbon atom is about 0.01~0.07 μ_B, and the total molecular magnetic moment is about 0.2~0.3 μ_B. The small magnetic moment per mole in our samples is due to very small magnetic moment on each naphthalene unit. This is very different from inorganic materials, where each unpaired electron can form a magnetic moment of 1 μ_B. Owing to the presence of non-magnetic materials in the intercalated samples, such as KH, the experimentally fitted magnetic moment is smaller than the theoretical value.

The energy band of the theoretical model is shown in Figure 3b. The presence of electronic states on the Fermi level indicates that the theoretical structure is metallic. Figure 3c,d presents partial density of states (PDOS) and spin-dependent density of states (DOS) of the theoretical model in the ferromagnetic configuration, respectively. The PDOS suggests that the C-2p orbital makes the main contribution to the state near the Fermi level, and the contribution of the C-2s and K-4s orbitals is very small, indicating that electrons are transferred from the K-4s orbital to the π-orbital of 2,7-DMN. On account of the near degeneracy between ferromagnetic and antiferromagnetic configurations, the density of states with spin down and up near the Fermi level is almost symmetric, as shown in Figure 3d [12]. The summation of DOS of spin down and up in Figure 3d is basically the same as PDOS of C-2p orbital in Figure 3c, suggesting that C-2p orbital is the main source of magnetism generation in potassium-intercalated 2,7-DMN. The metallic behavior of the structure can also be verified from DOS and PDOS near the Fermi level.

3.3. Raman Spectroscopy of Pristine and Potassium-Intercalated 2,7-DMN

The variation information of 2,7-DMN molecule before and after potassium intercalation was carried out by Raman spectroscopy. Pristine 2,7-DMN has a total of 66 Raman vibration modes which can be roughly divided into C-H stretching, C-C stretching, C-C bending, C-H bending, ring bending and methyl group vibrations, etc. All the vibration modes of pristine organics shown in Figure 4 are basically consistent with those of 2,7-DMN reported in the literature [46]. The two modes at 143 and 468 cm^{-1} belong to the ring torsional bending. The two modes at 421 and 444 cm^{-1} involve the ring in-plane bending. The mode at 773 cm^{-1} involves the C-H out of plane bending. The two modes at 1177 and 1384 cm^{-1} involve the C-H in-plane bending. The two modes at 1464 and 1545 cm^{-1} are assigned to the C-C stretching. The mode at 1572 cm^{-1} is assigned to the CH$_3$ out of plane bending [46].

When potassium is intercalated into 2,7-DMN, the vibration modes of the two samples change significantly. The two modes in pristine 2,7-DMN at 143 and 444 cm^{-1} disappear, while the two modes at 1464 and 1572 cm^{-1} remain the same. In addition, the modes at 421, 468, 773, 1177, 1384, and 1545 cm^{-1} red-shift by 6, 15, 25, 11, 24, and 20 cm^{-1}, respectively. This red-shift phenomenon which can be explained by phonon softening effect reveals a clear signature of charge transfer to organic molecules and is also found in other metal-intercalated PAHs [47,48], GICs [49], C$_{60}$ [50] and carbon nanotube [51]. It is worth noting that novel physical properties such as superconductivity or ferromagnetism have been found in all of these donor-intercalated organic materials with π-molecular orbitals, suggesting that the charge transfer injects conduction electrons into the organic [52].

The interaction between potassium atoms and organic molecules mainly manifests in the low frequency vibration region of the Raman spectrum, due to relatively heavy mass of K and weaker interaction compared to C-C bond. Because the crystallinity of the metal intercalation sample is not good enough, it is difficult to distinguish the detailed changes of the structure from the Raman spectroscopy data in the low frequency region. It

was found that the interaction between potassium and organic materials will suppress the lattice vibration and also cause the peak to broaden [50].
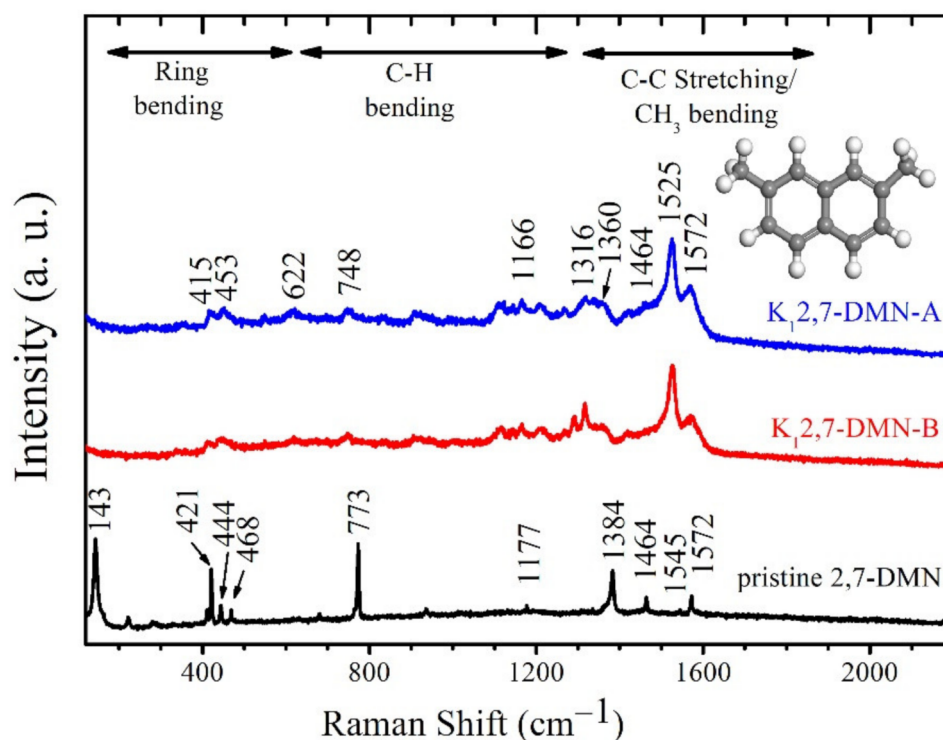

Figure 4. Raman spectroscopy of pristine and potassium-intercalated 2,7-DMN samples collected at room temperature.

4. Conclusions

In this study, thermostatic ultrasound and low-temperature annealing were used to prepare potassium-intercalated 2,7-DMN molecule crystal materials. Magnetic measurement showed that all the samples with potassium intercalation exhibited Curie paramagnetism, and the maximum magnetic moment was 0.15 $\mu_B \cdot$mol^{-1}. Combined with X-ray diffraction and first-principles calculations, it was found that potassium and 2,7-DMN formed a stable new intercalated structure according to the molar ratio of 1:2. The calculation results show that the intercalated structure should be metallic and has local magnetic moment, but the magnetic interaction between the molecules is very small, leading to the paramagnetic behavior in the samples. The red-shift phenomenon in Raman spectrum also confirmed that intercalation induced the 4s electron transfer of potassium, which was the source of the local magnetic moment in the samples.

Potassium-intercalated triphenylene showed Curie paramagnetism, while sodium-intercalated triphenylene exhibited superconductivity [38]. Similar differentiation was also found in A_xC_{60} (A = K, Rb, Cs) [53]. In potassium-intercalated picene, it was theoretically predicted that an increase of volume by 10% can enhance the local magnetic moment and antiferromagnetic order, while a 10% decrease in volume favors a nonmagnetic state with zero local magnetic moment. These results suggest that the physical properties of alkali-metal-intercalated organic materials are very sensitive to the distance between molecules [54]. In potassium-intercalated 2,3-DMN, the average occupied volume of each molecule is 235.75 Å^3, while in potassium-intercalated 2,7-DMN, this value becomes 258.1 Å^3, indicating that the molecular spacing is slightly larger for the latter case. This may be the cause of the magnetic moment in the potassium-intercalated 2,7-DMN sample. Therefore, the decoration of PAHs with organic functional groups in the appropriate positions opens a new way for the research of new organic magnetic and superconducting materials.

References

1. Radovic, L.R. Probing the 'elephant': On the essential difference between graphenes and polycyclic aromatic hydrocarbons.
Carbon **2021**, *171*, 798–805. [CrossRef]
2. Wang, N.; Zhi, Y.; Wei, Y.; Zhang, W.; Liu, Z. Molecular elucidating of an unusual growth mechanism for polycyclic aromatic
hydrocarbons in confined space. *Nat. Commun.* **2020**, *11*, 1079. [CrossRef]
3. Tan, D.; Jin, J.; Guo, C.; Chen, D.J. Magnetic magnesium oxide composites for rapid removal of polycyclic aromatic hydrocarbons
and cadmium ions from water. *Environ. Chem.* **2020**, *17*, 479–487. [CrossRef]
4. Mu, Q.; Shiraiwa, M.; Octaviani, M.; Ma, N.; Ding, A.; Su, H.; Lammel, G.; PoSchl, U.; Heng, Y. Temperature effect on phase state
and reactivity controls atmospheric multiphase chemistry and transport of PAHs. *Sci. Adv.* **2018**, *4*, eaap7314. [CrossRef]
5. Rajasekhar, B.; Nambi, I.M.; Govindarajan, S.K. Human health risk assessment of ground water contaminated with petroleum
PAHs using Monte Carlo simulations: A case study of an Indian metropolitan city. *J. Environ. Manag.* **2018**, *205*, 183–191.
[CrossRef] [PubMed]
6. Wentworth, G.R.; Aklilu, Y.A.; Landis, M.S.; Hsu, Y.M. Impacts of a large boreal wildfire on ground level atmospheric concentra-
tions of PAHs, VOCs and ozone. *Atmos. Environ.* **2018**, *178*, 19–30. [CrossRef]
7. Maigorzata, R.; Kinga, K.; Lekhanath, K.; Gabriela, B.N.; Marta, S.; Mariusz, M.; Katarzyna, C.; Halina, P.; Bozena, Z.; Jacek, N.
Homogeneity study of candidate reference material (contaminated soil) based on determination of selected metals, pcbs and
pahs. *Measurement* **2018**, *128*, 1–12.
8. Shi, W.; Guo, Y.; Liu, Y. When flexible organic field-effect transistors meet biomimetics: A prospective view of the internet of
things. *Adv. Mater.* **2019**, *32*, 1901493. [CrossRef] [PubMed]
9. Kang, S.; Huh, J.S.; Kim, J.J.; Park, J. Highly efficient deep-blue fluorescence OLEDs with excellent charge balance based on
phenanthro[9,10-d]oxazole-anthracene derivatives. *J. Mater. Chem. C* **2020**, *8*, 11168–11176. [CrossRef]
10. Yagui, J.; Angel, F.A. Benzodithiophene-based small molecules for vacuum-processed organic photovoltaic devices. *Opt. Mater.*
2020, *109*, 110354. [CrossRef]
11. Mitsuhashi, R.; Suzuki, Y.; Yamanari, Y.; Mitamura, H.; Kambe, T.; Ikeda, R.; Okamoto, H.; Fujiwara, A.; Yamaji, M.; Kawasaki, N.
Superconductivity in alkali-metal-doped picene. *Nature* **2010**, *464*, 76–79. [CrossRef]
12. Fu, M.A.; Wang, R.S.; Yang, H.; Zhang, P.Y.; Zhang, C.F.; Chen, X.J.; Gao, Y.; Huang, Z.B. π-electron weak ferromagnetism in
potassium-intercalated 9-phenylanthracene. *Carbon* **2021**, *173*, 587–593. [CrossRef]
13. Nakagawa, T.; Yuan, Z.; Zhang, J.; Yusenko, K.V.; Jin, C. Structure and magnetic property of potassium intercalated pentacene:
Observation of superconducting phase in KxC22H14. *J. Phys. Condens. Matter.* **2016**, *28*, 484001. [CrossRef]
14. Zhong, G.H.; Huang, Z.B.; Lin, H.Q. Antiferromagnetism in Potassium-Doped Polycyclic Aromatic Hydrocarbons. *IEEE Trans.
Magn.* **2014**, *50*, 1700103. [CrossRef]
15. Takabayashi, Y.; Menelaou, M.; Tamura, H.; Takemori, N.; Prassides, K. π-Electron S = 1/2 Quantum Spin-Liquid State in an Ionic
Polyaromatic Hydrocarbon. *Nat. Chem.* **2017**, *9*, 635–643. [CrossRef] [PubMed]
16. Štefančič, A.; Klupp, G.; Knaflič, T.; Yufit, D.S.; Tavčar, G.; Potočnik, A.; Beeby, A.; Arčon, D. Triphenylide-based molecular
solid—A new candidate for a quantum spin-liquid compound. *J. Phys. Chem. C* **2017**, *121*, 14864–14871. [CrossRef]

17. Phan, Q.; Heguri, S.; Tanabe, Y.; Shimotani, H.; Nakano, T.; Nozue, Y.; Tanigaki, K. Tuning of the ground state in electron doped anthracene. *Dalton Trans.* **2014**, *43*, 10040–10045. [CrossRef]

18. Heguri, S.; Kobayashi, M.; Tanigaki, K. Questioning the existence of superconducting potassium doped phases for aromatic hydrocarbons. *Phys. Rev. B* **2015**, *92*, 014502. [CrossRef]

19. Romero, F.D.; Pitcher, M.J.; Hiley, C.I.; Whitehead, G.; Kar, S.; Ganin, D.; Antypov, A.Y.; Collins, C.; Dyer, M.S.; Klupp, G. Redox-controlled potassium intercalation into two polyaromatic hydrocarbon solids. *Nat. Chem.* **2017**, *9*, 644–652. [CrossRef]

20. Zhong, G.H.; Yang, D.Y.; Zhang, K.; Wang, R.S.; Zhang, C.; Lin, H.Q.; Chen, X.J. Superconductivity and Phase Stability of Potassium-Doped Biphenyl. *Phys. Chem. Chem. Phys.* **2018**, *20*, 25217–25223. [CrossRef]

21. Wang, R.S.; Gao, Y.; Huang, Z.B.; Chen, X.J. Superconductivity above 120 Kelvin in a Chain Link Molecule. *arXiv* **2017**, arXiv:1703.06641.

22. Yan, J.F.; Zhong, G.H.; Wang, R.S.; Zhang, K.; Lin, H.Q.; Chen, X.J. Superconductivity and Phase Stability of Potassium-Intercalated p-Quaterphenyl. *J. Phys. Chem. Lett.* **2018**, *10*, 40–47. [CrossRef]

23. Huang, G.; Zhong, G.H.; Wang, R.S.; Han, J.X.; Lin, H.Q.; Chen, X.J. Superconductivity and phase stability of potassium-doped p-quinquephenyl. *Carbon* **2019**, *143*, 837–843. [CrossRef]

24. Wang, X.F.; Liu, R.H.; Gui, Z.; Xie, Y.L.; Yan, Y.J.; Ying, J.J.; Luo, X.G.; Chen, X.H. Superconductivity at 5 K in Alkali-Metal-Doped Phenanthrene. *Nat. Commun.* **2012**, *2*, 507.

25. Wang, X.F.; Yan, Y.J.; Gui, Z.; Liu, R.H.; Chen, X.H. Superconductivity in A 1.5 phenanthrene (A = Sr, Ba). *Phys. Rev. B* **2011**, *84*, 214523.

26. Teranishi, K.; He, X.; Sakai, Y.; Izumi, M.; Goto, H.; Eguchi, R.; Takabayashi, Y.; Kambe, T.; Kubozono, Y. Observation of zero resistivity in K-doped picene. *Phys. Rev. B* **2013**, *87*, 060505.

27. Kubozono, Y.; Mitamura, H.; Lee, X.; He, X.; Yamanari, Y.; Takahashi, Y.; Suzuki, Y.; Kaji, Y.; Eguchi, R.; Akaike, K. Metal-intercalated aromatic hydrocarbons: A new class of carbon-based superconductors. *Phys. Chem. Chem. Phys.* **2011**, *13*, 16476–16493.

28. Xue, M.; Cao, T.; Wang, D.; Wu, Y.; Yang, H.; Dong, X.; He, J.; Li, F.; Chen, G.F. Superconductivity above 30 K in Alkali-Metal-Doped Hydrocarbon. *Sci. Rep.* **2012**, *2*, 389.

29. Marik, A.; Kumar, C.; Mohakud, S. Compensated Ferrimagnetism and Half Metallic Behavior in Potassium(K) Intercalated Naphthalene. *Phys. Status Solidi B* **2020**, *257*, 2000398.

30. Peng, D.; Wang, R.S.; Chen, X.J. Superconductivity in Sodium Potassium Alloy Doped 2,2′-Bipyridine from Near Room Temperature Synthesis. *J. Phys. Chem. C* **2020**, *124*, 906–912. [CrossRef]

31. Wang, R.S.; Cheng, J.; Wu, X.L.; Yang, H.; Chen, X.J.; Gao, Y.; Huang, Z.B. Superconductivity at 3.5 K and/or 7.2 K in Potassium-Doped Triphenylbismuth. *J. Chem. Phys.* **2018**, *149*, 144502. [CrossRef]

32. Wang, R.S.; Yang, H.; Cheng, J.; Wu, X.L.; Fu, M.A.; Chen, X.J.; Gao, Y.; Huang, Z.B. Discovery of Superconductivity in Potassium-Doped Tri-p-Tolylbismuthine. *J. Phys. Chem. C* **2019**, *123*, 19105–19111. [CrossRef]

33. Wang, R.S.; Chen, L.C.; Yang, H.; Fu, M.A.; Cheng, J.; Wu, X.L.; Gao, Y.; Huang, Z.B.; Chen, X.J. Superconductivity in an Organometallic Compound. *Phys. Chem. Chem. Phys.* **2019**, *21*, 25976–25981. [CrossRef] [PubMed]

34. Valentí, R.; Winter, S.M. Polycyclic aromatic hydrocarbons: Synthesis successes. *Nat. Chem.* **2017**, *9*, 608–609. [CrossRef]

35. Spisak, S.N.; Rogachev, A.Y.; Zabula, A.V.; Filatov, A.S.; Clérac, R.; Petrukhina, M.A. Tuning the separation and coupling of corannulene trianion-radicals through sizable alkali metal belts. *Chem. Sci.* **2017**, *8*, 3137–3145. [CrossRef]

36. Guijarro, A.; Verges, J.A. Prediction of a metallic phase for Cs3Pentacene compound. *Mater. Res. Express* **2018**, *5*, 066554. [CrossRef]

37. Zhang, J.; Whitehead, G.; Manning, T.D.; Stewart, D.; Hiley, C.; Pitcher, M.J.; Jansat, S.; Prassides, K.; Rosseinsky, M.J. The reactivity of solid rubrene with potassium: Competition between intercalation and molecular decomposition. *J. Am. Chem. Soc.* **2018**, *140*, 18162–18172. [CrossRef]

38. Yoon, T.; Park, I.; Nguyen, T.P.; Kim, D.Y.; Choi, H.C. Discovery of sodium-doped triphenylene superconductor through searching the organic material database. *Chem. Mater.* **2020**, *32*, 3358–3364. [CrossRef]

39. Wu, X.L.; Wang, R.S.; Yang, H.; Zhang, J.; Fu, M.A.; Fang, S.C.; Chen, X.J.; Gao, Y.; Huang, Z.B. Structural and Magnetic Properties of Potassium-Doped 2,3-DiMethylnaphthalene. *Crystals* **2021**, *11*, 608. [CrossRef]

40. Kresse, G.; Furthmuller, J. Efficient iterative schemes for ab initio total-energy calculations using a plane-wave basis set. *Phys. Rev. B* **1996**, *54*, 11169–11186. [CrossRef]

41. Perdew, J.P.; Burke, K.; Ernzerhof, M. Generalized gradient approximation made simple. *Phys. Rev. Lett.* **1996**, *77*, 3865–3868. [CrossRef] [PubMed]

42. Blchl, P.E. Projector augmented-wave method. *Phys. Rev. B* **1994**, *50*, 17953–17979. [CrossRef] [PubMed]

43. Fujiwara, M.; Chidiwa, T.; Tanimoto, Y. Magnetic Orientation under Gravity: Biphenyl and Naphthalene Crystals. *J. Phys. Chem. B* **2000**, *104*, 8075–8079. [CrossRef]

44. Lapidus, S.; McConnell, A.; Stephens, P.; Miller, J. Structure and magnetic ordering of a 2-D $Mn^{II}(TCNE)I(OH_2)$ (TCNE = tetracyanoethylene) organic-based magnet (Tc = 171 K). *Chem. Commun.* **2011**, *47*, 7602–7604. [CrossRef] [PubMed]

45. Zhang, B.; Zhang, Y.; Zhu, D. $(BEDT-TTF)_3Cu_2(C_2O_4)_3(CH_3OH)_2$: An organic-inorganic hybrid antiferromagnetic semiconductor. *Chem. Commun.* **2012**, *48*, 197–199. [CrossRef] [PubMed]

46.   Rao, D.J.; Ramakrishna, Y.; Padmarao, C.V.; Rao, B.V. Vibrational spectroscopic study of 2,6- and 2,7-dimethylnaphthalenes by Density functional theory. *Int. J. Adv. Res. Sci. Technol.* **2012**, *1*, 135–159.

47.   Kambe, T.; He, X.; Takahashi, Y.; Yamanari, Y.; Teranishi, K.; Mitamura, H.; Shibasaki, S.; Tomita, K.; Eguchi, R.; Goto, H.; et al. Synthesis and physical properties of metal-doped picene solids. *Phys. Rev. B* **2012**, *86*, 214507. [CrossRef]

48.   Huang, Q.W.; Zhong, G.H.; Zhang, J.; Zhao, X.M.; Zhang, C.; Lin, H.Q.; Chen, X.J. Constraint on the potassium content for the superconductivity of potassium-intercalated phenanthrene. *J. Chem. Phys.* **2014**, *140*, 114301. [CrossRef]

49.   Dresselhaus, M.S.; Dresselhaus, G. Intercalation compounds of graphite. *Adv. Phys.* **1981**, *30*, 139–326. [CrossRef]

50.   Zhou, P.; Wang, K.A.; Eklund, P.C.; Dresselhaus, G.; Dresselhaus, M.S. Raman-scattering study of the electron-phonon interaction in M_3C_{60} (M = K, Rb). *Phys. Rev. B* **1993**, *48*, 8412–8417. [CrossRef]

51.   Rao, A.M.; Eklund, P.C.; Bandow, S.; Thess, A.; Smalley, R.E. Evidence for charge transfer in doped carbon nanotube bundles from Raman scattering. *Nature* **1997**, *388*, 257–259. [CrossRef]

52.   Kubozono, Y.; Eguchi, R.; Goto, H.; Hamao, S.; Kambe, T.; Terao, T.; Nishiyama, S.; Zheng, L.; Miao, X.; Okamoto, H. Recent progress on carbon-based superconductors. *J. Phys. Condens. Matter.* **2016**, *28*, 334001. [CrossRef]

53.   Fleming, R.M.; Ramirez, A.P.; Rosseinsky, M.J.; Murphy, D.W.; Haddon, R.C.; Zahurak, R.M.; Makhija, A.V. Relation of structure and superconducting transition temperature in A_3C_{60}. *Nature* **1991**, *352*, 787–788. [CrossRef]

54.   Zhong, G.H.; Zhang, C.; Wu, G.F.; Huang, Z.B.; Chen, X.J.; Lin, H.Q. First-principles investigations on the magnetic property in tripotassium doped picene. *J. Appl. Phys.* **2013**, *113*, 76. [CrossRef]